Ocean-bottom ultralow-frequency (ULF) seismo-acoustic ambient noise: 0.002 to 0.4 Hz

George H. Sutton and Noël Barstow
Rondout Associates, Incorporated, P. O. Box 224, Stone Ridge, New York 12484

(Received 24 November 1989; accepted for publication 29 December 1989)

Observed spatial and temporal characteristics of ultralow-frequency (ULF) ocean-bottom seismo-acoustic ambient noise are required in order to construct realistic quantitative predictive models of the phenomena involved. Few such data exist or have been studied, especially for frequencies below about 0.1 Hz. Analysis of noise data is presented in the band 0.002 to 0.4 Hz from a 2-week period, 11/28–12/12/67, recorded from long-period, three-component seismometers and a hydrophone of the Columbia-Point Arena ocean-bottom seismic station (OBSS, 38° 09.2′N–124° 54.4′W, 3903-m depth). Two intense NE Pacific storms with hurricane force winds occurred during the emphasized time period. Time variations of spectra and of amplitude and phase coherencies of the four-component OBSS data are related to the storm histories and to local weather/wave conditions and are used to identify motion (seismic wave) types and directions of propagation.

PACS numbers: 43.30.Nb

INTRODUCTION

The general objective of this research is to improve our quantitative understanding of the ambient acoustic/seismic noise field in the ocean as a function of location and time in the ultralow-frequency (ULF) (0.001 to 1 Hz)/very low-frequency (VLF) (1 to 50 Hz) frequency band by identifying and characterizing the noise sources and determining the propagation characteristics of the ambient noise field as functions of the ocean and sub-bottom environmental parameters. The specific research reported here characterizes ULF ocean-bottom noise during two northeast Pacific storms, measured at a single multisensor station.

The most extensive set of ocean bottom data on long period seismic background noise and signals was obtained from the Columbia-Point Arena ocean-bottom seismic station (OBSS, Sutton *et al.*, 1965). OBSS was installed on 18 May 1966 at 38° 09.2′N, 124° 54.4′W about 200 km west of San Francisco at a depth of 3903 m, and it was in continuous operation for more than 6 years, until 11 September 1972. Though a number of papers (e.g., Auld *et al.*, 1969; Latham and Nowroozi, 1968; Piermattei and Nowroozi, 1969; Sutton *et al.*, 1965; Nowroozi *et al.*, 1968, 1969) have been published using OBSS data, little had been published on the background noise, especially outside the principal microseism band, 0.1 to 0.2 Hz, until recent interest in ULF/VLF noise led us to examine OBSS data specifically for this information. OBSS instruments primarily used for this study are the Lamont long-period (LP) triaxial seismometer (15-s natural period, originally developed for lunar use) and the long-period (crystal) hydrophone. Records from the three-component short-period (SP) system (1-s natural period) and short-period (coil-magnet) hydrophone also were consulted. We digitized FM tapes of the long-period data at 8 spikes/s.

We present analyses of OBSS seismo-acoustic ULF data for a 2-week period, 11/28 to 12/11/67, during which two NE Pacific storms with hurricane force winds occurred. Samples of ocean-bottom noise in the frequency band 0.002 to 0.4 Hz are analyzed for coherency and amplitude and phase relationships among the three components of particle motion and pressure.

I. RESULTS

Figure 1 shows the location and the orientation of the horizontal components of OBSS and the tracks of the two storms studied. Maximum intensities of storm activity occurred between about 1200 UT 12/1 and 1800 UT 12/2 for the earlier storm and between about 1200 UT 12/5 and 0000 UT 12/6 for the later storm (Mariners' Weather Log, 1968). From 11/30 through 12/8 (except 12/2) swell height near OBSS was greater than 15 ft and on 11/30 and 12/3–12/5 combined sea and swell was greater than 20 ft (historical conditions obtained from Pacific Weather Analysis). For the period 11/28–12/11/67, we digitized, somewhat arbitrarily, 6-, 12-, or 4-h samples of noise (Fig. 2). These samples of ocean-bottom noise are used to determine spectra, coherency, and amplitude and phase relationships among the three components of particle motion and pressure in the frequency band 0.002–0.4 Hz. Below about 0.003 Hz, some low-amplitude samples may be affected by system noise.

The pressure spectra generally agree with those obtained by Cox *et al.* (1984) and Webb and Cox (1986) showing a strong minimum between about 0.03 and 0.1 Hz referred to as the "noise notch"; motion spectra from the OBSS seismometers, especially the vertical sensor, are qualitatively similar to the pressure spectra (Fig. 3). Figure 3 shows velocity and pressure spectra from three different times: Time 1 (0200 UT 11/28) is before the storms; time 2 (1200 UT 12/4) occurs after the peak in double-frequency (twice ocean swell frequency) microseisms associated with storm 1; and time 3 (0200 UT12/8) is near the peak double-frequency microseisms associated with storm 2. It can be

 0001-4966/90/052005-08$00.80

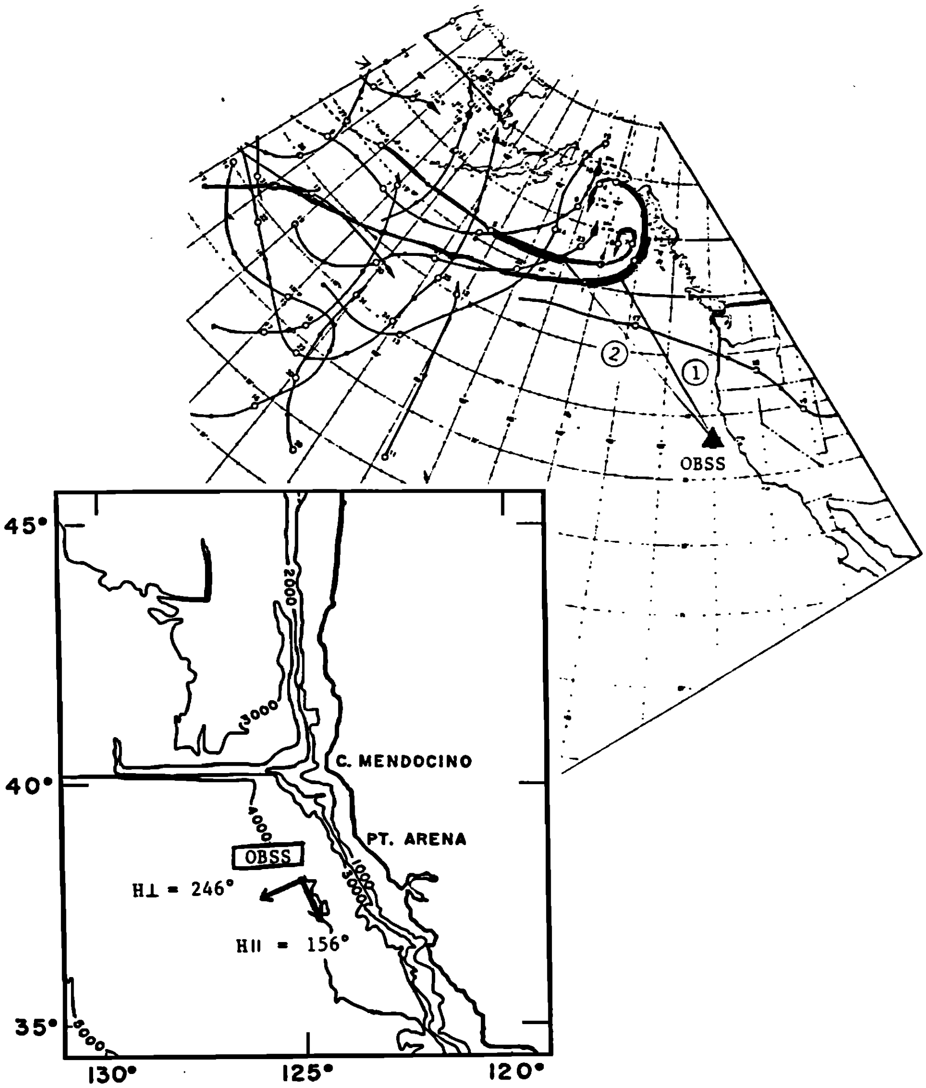

FIG. 1. Location and orientation of OBSS and tracks of two 1967 hurricanes. Thickened lines show duration and location along the storm tracks of huricane force winds. Storm 1 (11/29–12/5); closest approach of center of hurricane winds; $\Delta = 15.7°$. Storm 2 (12/3–12/8); closest approach of hurricane winds; $\Delta = 19.3°$.

seen that the whole spectral level between 0.003 and 0.4 Hz is raised for both vertical velocity $\dot{Z}$ and pressure P. For frequencies below about 0.08 Hz, the horizontal components are affected more by local tidal currents (most likely from direct turbulent pressure on the OBSS package—Sutton, 1986; Sutton and Duennebier, 1987, 1989) than by the storm activity.

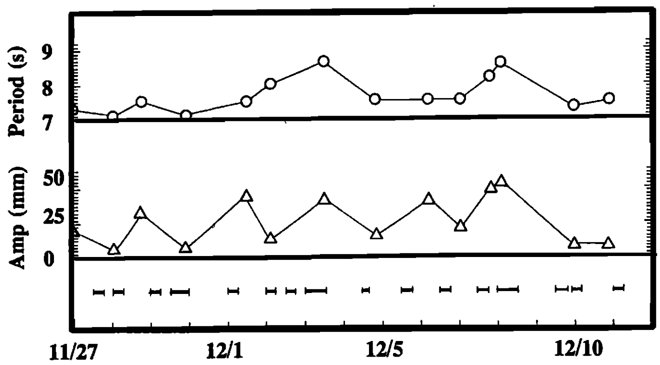

FIG. 2. Measured from the original long-period photographic, continuous analog records are predominant period (circles) and average peak–peak trace amplitude (triangles) for vertical component microseismic background noise during times of amplitude maxima and minima (usually lasting several hours). Horizontal bars represent time samples of background noise digitized from original FM tapes.

The data divide naturally into five frequency bands (0.004–0.02 Hz, 0.02–0.04 Hz, 0.04–0.08 Hz, 0.08–0.2 Hz, and 0.2–0.4 Hz) based upon observed characteristics and upon assumed mode of origin and/or propagation. The band divisions are labeled in Fig. 4, where amplitude and phase coherency between pressure and vertical motion are shown. Below, we discuss each band separately.

A. Band 0.004–0.02 Hz

In this band, it is believed that the pressure variations result from long gravity water waves having wavelengths greater than water depth, but much less than seismic waves of the same frequency (Webb and Cox, 1986; Webb, 1988; Barstow *et al.*, 1989). Webb and Cox (1986) predict that this band should be fairly constant with time; however, we observe an increase in P and Z near 0.01 Hz of about 20 dB during the storms (Fig. 3). Sutton *et al.* (1965) also found a temporal correlation with ocean wave heights along the nearby (to OBSS) California coast. The pressure disturbance should produce a forced deformation of the bottom and, near 0.01 Hz, we observe a strong correlation between P

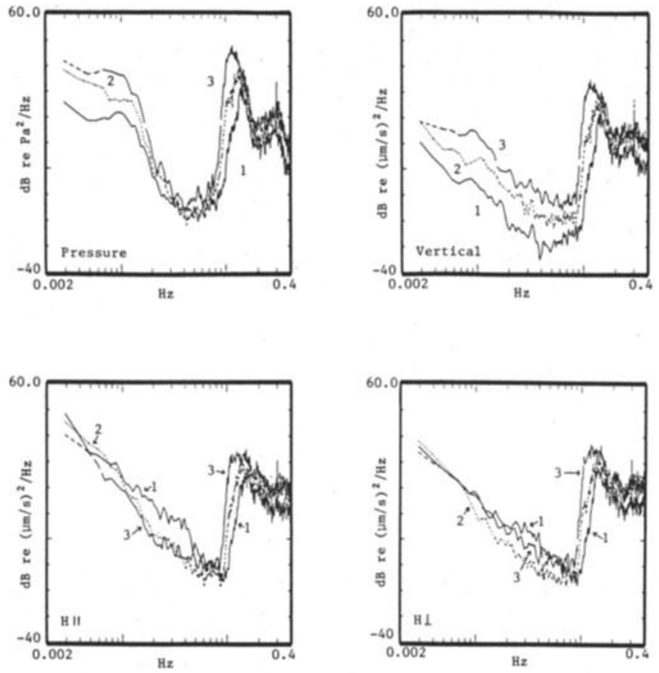

FIG. 3. Pressure and three-component velocity power spectra from three time periods: 1 before (11/28), 2 during (12/4), and 3 near a peak (12/8) in microseism storm activity associated with two NE Pacific hurricanes in December 1967. Note that the whole spectrum is raised for pressure and vertical motion and only that above 0.08 Hz for horizontal motion. Spectra were calculated from 1-h samples divided into eight Hanning windows with 62.5% overlap.

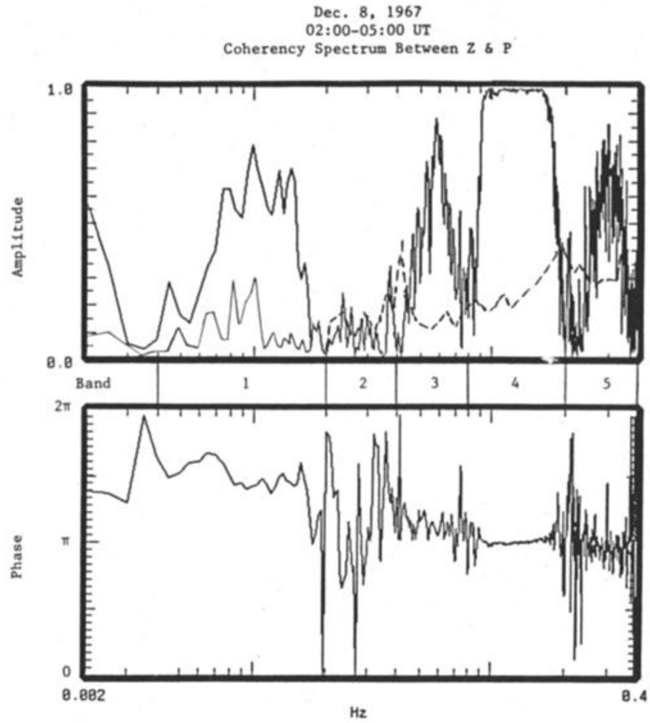

FIG. 4. Amplitude and phase coherency between vertical displacement and pressure during peak of microseism storm. An estimate of random amplitude coherency is given by the generally, lower amplitude spectrum obtained between samples of P and Z taken at separate times; above 0.02 Hz, the dashed line connects the largest maxima in the spectrum. The π phase (maximum pressure in phase with maximum down displacement) is correct for Rayleigh wave motion. Also, $3\pi/2$ phase near 0.01 Hz (maximum pressure in phase with maximum down velocity) is not consistent with simple static loading from long gravity water waves. Numbered frequency bands correspond to text. This and succeeding coherency spectra were calculated from 3-h samples divided into 16 Hanning windows with 62.5% overlap.

and Z in Figs. 4 and 5. Yamamoto and Torii (1986) use such correlated pressure and motion in shallow water to estimate rigidity versus depth in the sub-bottom as a function of gravity wavelength (period). This theory assumes that variations are slow enough that static loading theory is adequate. The approximately $3\pi/2$ phase between vertical displacement and pressure (maximum pressure in phase with maximum downward velocity) observed in Fig. 4 indicates that dissipation (radiation) is involved and that the static theory is not adequate. Static theory would predict π phase (maximum pressure in phase with maximum downward displacement) as is also the case for Rayleigh waves. The pressure-vertical velocity ratio ($P/\dot{Z}$) near 0.01 Hz is 24 dB $\pm$ 2.7 s.d. for 21 samples, much too large for fundamental mode Rayleigh waves. All $P/\dot{Z}$ ratios were obtained by graphical measurement of individual power spectra calculated from 1-hour samples divided into eight Hanning windows with 62.5% overlap.

B. Band 0.02–0.04 Hz

In this band, we observe poor P-Z coherence (Figs. 4 and 5). The $P/\dot{Z}$ ratio near 0.02 Hz is 13.2 dB $\pm$ 6.2 s.d. for 21 samples. This average is well above that expected for seismic waves. Near 0.04 Hz, however, some samples have ratios appropriate for fundamental mode Rayleigh waves (LR). During the storm, amplitudes near 0.04 Hz increased 10–20 dB (Fig. 3). In this band, which is partially within the 0.03–0.1-Hz "noise notch," some low-amplitude samples may be system noise limited.

C. Band 0.04–0.08 Hz

P-Z coherence is variable in this band, which is also within the 0.03- to 0.1-Hz noise notch (Figs. 4 and 5). During the storm, amplitudes near 0.06 Hz increased 10–15 dB. The $P/\dot{Z}$ ratio near 0.06 Hz for 21 samples is 6.8 dB $\pm$ 3.1 s.d.; again, some low-amplitude samples may be system noise limited. The highest amplitude samples (Fig. 6) have amplitude and phase relationships consistent with fundamental mode Rayleigh waves.

This is the frequency band of single-frequency microseisms and of prominent oceanic Rayleigh waves from earthquakes. The single-frequency microseisms are generally believed to be produced from direct pressure of shoaling swell in coastal areas and have been observed mostly on land instruments (Oliver, 1962; Oliver and Page, 1963; Haubrich and McCamy, 1963; Cessaro and Chan, 1989). Consistent with this are Webb and Constable's (1986) interpretation of ambiguous results from a two-element ocean-bottom array as indicating Rayleigh propagation from near shore. Spectra (peaking near 0.06 Hz) and coherencies observed from June 1966 OBSS data by Barstow *et al.* (1989), however, clearly indicate fundamental mode Rayleigh waves propagating

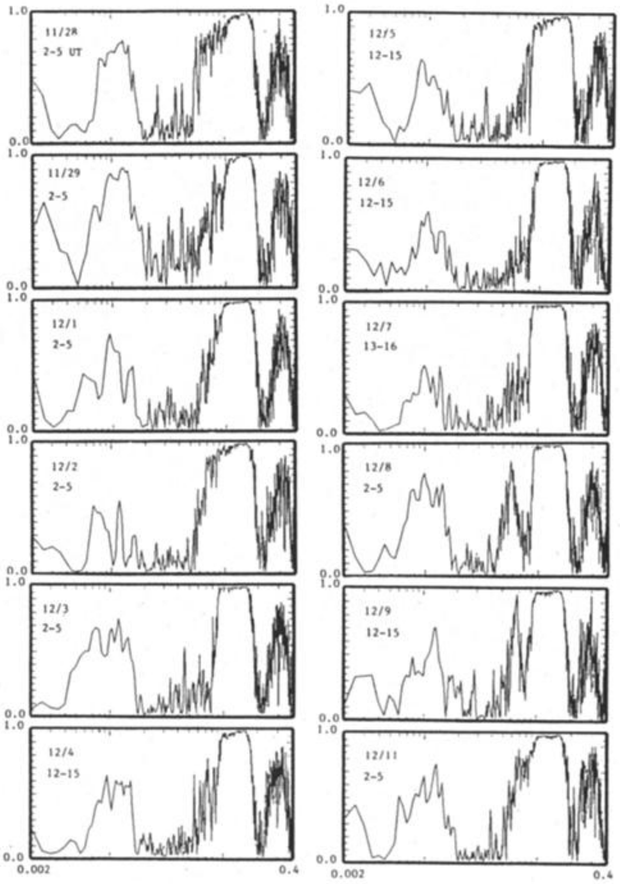

FIG. 5. Amplitude coherency between pressure and vertical motion (0.002 to 0.4 Hz) during 2-week period including two hurricanes. Note the variable coherency in the "single-frequency" microseism band between about 0.05 and 0.1 Hz and the consistently low coherency near 0.2 Hz and also from 0.02–0.04 Hz.

shoreward rather than seaward, as would be expected from generation near the California coast.

Webb and Cox (1986) noted the transient nature of spectral peaks for ocean-bottom single-frequency microseisms compared to more stable double-frequency microseisms. We observe generally strong but variable *P-Z* coherency during the 11/28–12/11/67 time period, but there are few clear spectral peaks in this bandwidth. However, within the 3-h period of high *P-Z* coherency near 0.06 Hz (0200-0500 UT 12/8, Fig. 5), we are able to observe single-frequency microseisms by narrow bandpass filtering the seismograms (Fig. 7). These microseisms, peaked at 0.05–0.06 Hz, have proper amplitude and phase relationships for LR and indicate shoreward (from 260°) propagation, as did our earlier results (Barstow *et al.*, 1989). Also, we do not observe a precise 2 to 1 frequency relationship with the observed double-frequency microseisms as would be expected if the same swell produced both types. Oliver and Page (1963) and Haubrich and McCamy (1963), for example, at land stations observed a quite accurate 2 to 1 relationship.

D. Band 0.08–0.2 Hz

This is the band of the prominent double-frequency microseisms. We observe high *P-Z* coherency and a large increase in amplitude (30–40 dB) and an increase in period during the storms (Figs. 2 and 3). The $P/\dot{Z}$ ratio near 0.1 Hz is 15.2 dB $\pm$ 0.8 s.d. for 21 samples. The amplitude and phase relationships in this band indicate fundamental mode Rayleigh waves propagating shoreward assuming prograde motion based on an appropriate velocity structure (Latham and Nowroozi, 1968; Bradner and Latham, 1972). The evidence, least ambiguous for double-frequency microseisms, is as follows. (The same kinds of data and reasoning were used to characterize single-frequency microseisms and will be discussed for wind-wave microseisms.) The π phase difference between pressure and vertical displacement is correct for Rayleigh wave motion and, though shown only in Fig. 4, we have observed it in all the coherence spectra between roughly 0.04 and 0.4 Hz (except at 0.08 and 0.2 Hz). The $P/\dot{Z}$ amplitude ratios from 0.04–0.15 Hz are consistent with fundamental mode Rayleigh waves for several reasonable velocity models (Fig. 6). The theoretical points on the $P/\dot{Z}$ ratio plots in Fig. 6 are from models 5 and 8 of Bradner, 1963. These models are probably the closest of those shown in Fig. 6 to the structure at OBSS (e.g., Sutton *et al.*, 1971); model values are given in Table I.

The H/Z amplitude ratios are also consistent with fundamental mode Rayleigh waves (Fig. 8). Velocity models

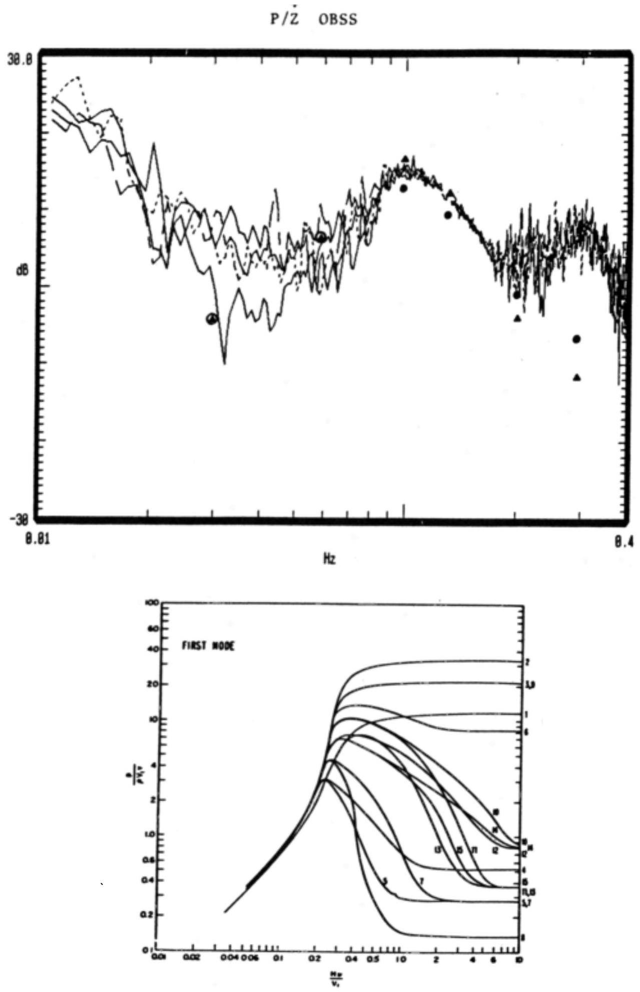

FIG. 6. Pressure-vertical velocity ratio for four time periods (12/2, 3, 5, 8) when both *P* and *Z* are at least 6 dB above the lowest recorded levels (i.e., little or no system noise). Theoretical curves are fundamental Rayleigh for different velocity models (Bradner, 1963). Triangles and circles on data plot are for models 8 and 5, respectively (Table I).

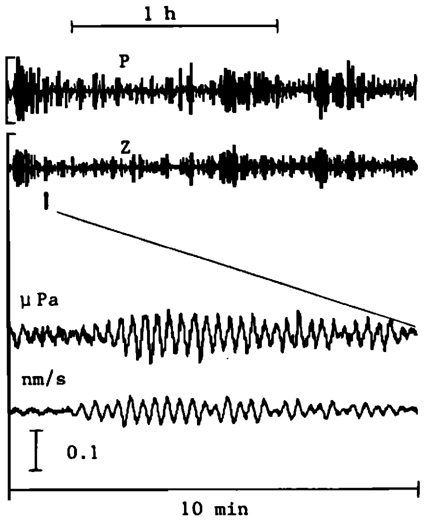

FIG. 7. Pressure and vertical velocity bandpass filtered from 0.04–0.06 Hz to enhance single-frequency microseisms; All traces start at 0300 UT on 12/8. Amplitude scale applies only to time-expanded traces, for which pressure is plotted positive downward.

appropriate for the OBSS site indicate prograde particle motion for LR at frequencies higher than about 0.1 Hz. Assuming prograde motion, then, the double-frequency microseisms are propagating shoreward (Fig. 9). In Fig. 9, the vertical to horizontal coherencies and transfer functions are used to determine the propagation direction of Rayleigh waves. The phase coherencies determine the appropriate quadrant and the ratio of the transfer functions determines the angle relative from $H\|$ (Fig. 1). Between 0.09 and 0.15 Hz (double-frequency), propagation is from the west (275°). In the same manner, we determined a propagation direction of 260° for single-frequency microseisms near 0.06 Hz, where fundamental mode LR is retrograde.

The relationship between the storms and the timing of changes in double-frequency microseisms is a clue to microseism origin. Using the distance to OBSS of the closest approach of hurricane force winds generated in storm 1 (Fig. 1), the calculated arrival time for 17-s water waves is 1200 UT on 12/3. Similarly for storm 2, the calculated arrival time is 2000 UT on 12/7. The earlier of two observed maxima for 8 1/2-s microseisms occurs at about 1200 UT 12/3 (Fig. 2), as predicted for generation near OBSS from interfering 17-s swell of storm 1. The later-occurring maximum

TABLE I. Bradner (1963) models 5 and 8.

Model no.	H,km	ρ,g/cm^3	V_s,km/s	V_p,km/s
5	6	1.03		1.52
	1	1.03	0.5	1.52
	6	2.75	3.98	6.9
	∞	3.09	4.68	8.1
8	6	1.03		1.52
	0.5	1.03	0.25	1.52
	1.5	2.54	2.77	4.8
	5	2.75	3.98	6.9
	∞	3.09	4.68	8.1

period and amplitude of double-frequency microseisms is observed early on 12/8, somewhat later than predicted for swell to reach OBSS from the distances of hurricane force winds associated with storm 2. It is important to our understanding of the generation of double-frequency microseisms that the observed high-amplitude, longest period arrivals from both storms are later than expected for Rayleigh waves generated either near the storm center or at the coastal areas nearest the storm center. Thus the time delay relative to the storm activity suggests double-frequency microseism generation near OBSS. We do not have a simple explanation for the 2- to 3-day cycle of double-frequency amplitude variations in Fig. 2. From 11/30–12/8, the low-amplitude values steadily increase, and then, on 12/10, they drop back to the prestorm low levels. The pattern of high-amplitude values is puzzling, yet the two longest-period peaks in amplitude sensibly relate to the storm tracks.

There have been many investigations, mostly involving only land observations, of double-frequency microseisms. They are generally believed to be generated by nonlinear wave–wave interaction either near a storm center or upon reflection from a coastline. Our ocean bottom data seem to require interaction offshore and away from the storm center. Perhaps the double-frequency microseisms from both storms are a result of interference between direct arriving storm swell and reflections off northern California and Oregon (Fig. 1).

E. Band 0.2–0.4 Hz

Figure 5 shows a stable P-Z coherency maximum near 0.3 Hz and a minimum near 0.2 Hz, separating it from the main double-frequency maximum. Amplitudes at 0.3 Hz varied up to 20 dB during the storms. Pressure and velocity amplitude fluctuations in this band correlate well with local wind and weather conditions; the generation of these microseisms is related to wind waves. On the original short-period photographic records, we observed two pronounced amplitude maxima, 12/3 and 12/7. These coincide with the two maxima in local winds indentified by Pacific Weather Analysis for the 2-week period studied: 30 n and above from the southeast and the northwest, respectively. The $P/\dot{Z}$ ratio near 0.3 Hz is 6.9 dB $\pm$ 1.0 s.d. for 16 samples. We note that observed $P/\dot{Z}$ ratios above about 0.15 Hz do not match fundamental mode theory well (Fig. 6). Higher modes change amplitude ratio and particle motion over narrow bandwidths and are highly sensitive to velocity structure, making it difficult to assess their propagation direction. If particle motion is prograde, propagation is seaward; i.e., from Fig. 9, near 0.33-Hz, propagation is from the east (100°). Relatively poor coherency between vertical and horizontal ground motion, however, suggests variable propagation direction.

II. SUMMARY

The pressure spectra are similar to those obtained by Cox *et al.* (1984) and Webb and Cox (1986) showing two maxima separated by a strong minimum between about

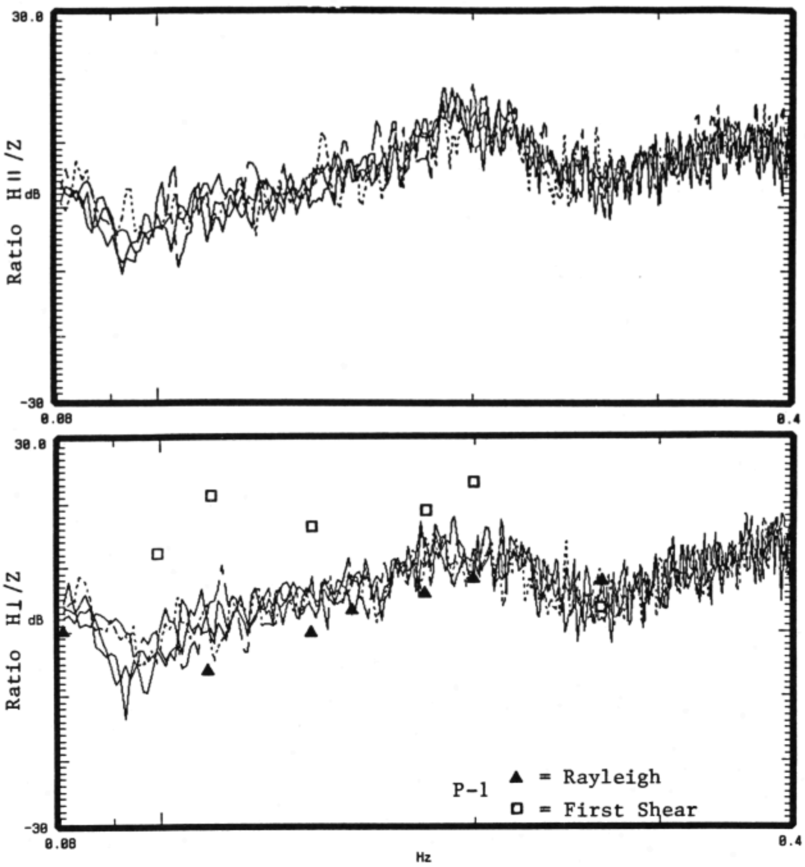

FIG. 8. Horizontal-vertical spectral ratios for same time periods as Fig. 6. Theoretical curves and points are from Latham and Nowroozi (1968); Positive ratio indicates retrograde motion and negative ratio indicates prograde motion.

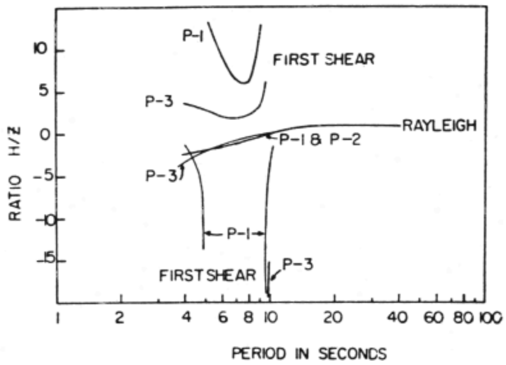

Layer Thickness, km	Compressional Velocity, km/s	Shear Velocity, km/s	Density, g/cc
	Model P-1		
3.800	1.51	0.00	1.03
0.010	1.51	0.15	1.65
0.100	1.60	0.19	1.70
0.100	1.71	0.37	1.79
0.100	1.80	0.53	1.86
0.200	1.90	0.70	1.90
0.500	2.20	1.10	2.05
1.400	4.70	2.70	2.54
4.600	6.90	3.98	2.90
∞	8.20	4.56	3.40

0.03–0.1 Hz; motion spectra from the OBSS seismometers, especially the vertical sensor, are similar to the pressure spectra. Coherent energy from 0.1–0.15 Hz, and intermittently near 0.06 Hz, indicate fundamental mode Rayleigh wave motion propagating shoreward. The timing of high-amplitude, longer-period double-frequency microseisms is consistent with microseism generation near OBSS rather than closer to the storm center. Background noise levels around 0.06 Hz are intermittently coherent between P and Z during the 2-week period of this study, but rarely do they produce spectral peaks. Coherent energy near 0.3 Hz is consistently high and the highest amplitudes correspond to the highest local winds for the period. The $P/\dot{Z}$ ratios show that these wind-wave microseisms are not fundamental mode Rayleigh waves.

Coherent energy near 0.01 Hz varies with time but is well above random coherency (estimated from coherency between samples of P and Z taken at separate times). Another result from both our previous study of fairly quiet conditions (Barstow *et al.*, 1989) and the current study of severe storm conditions is a 90° phase shift near 0.01 Hz between pressure and vertical displacement, indicating dissipation or radiation, in the forced deformation of the bottom from long gravity water waves.

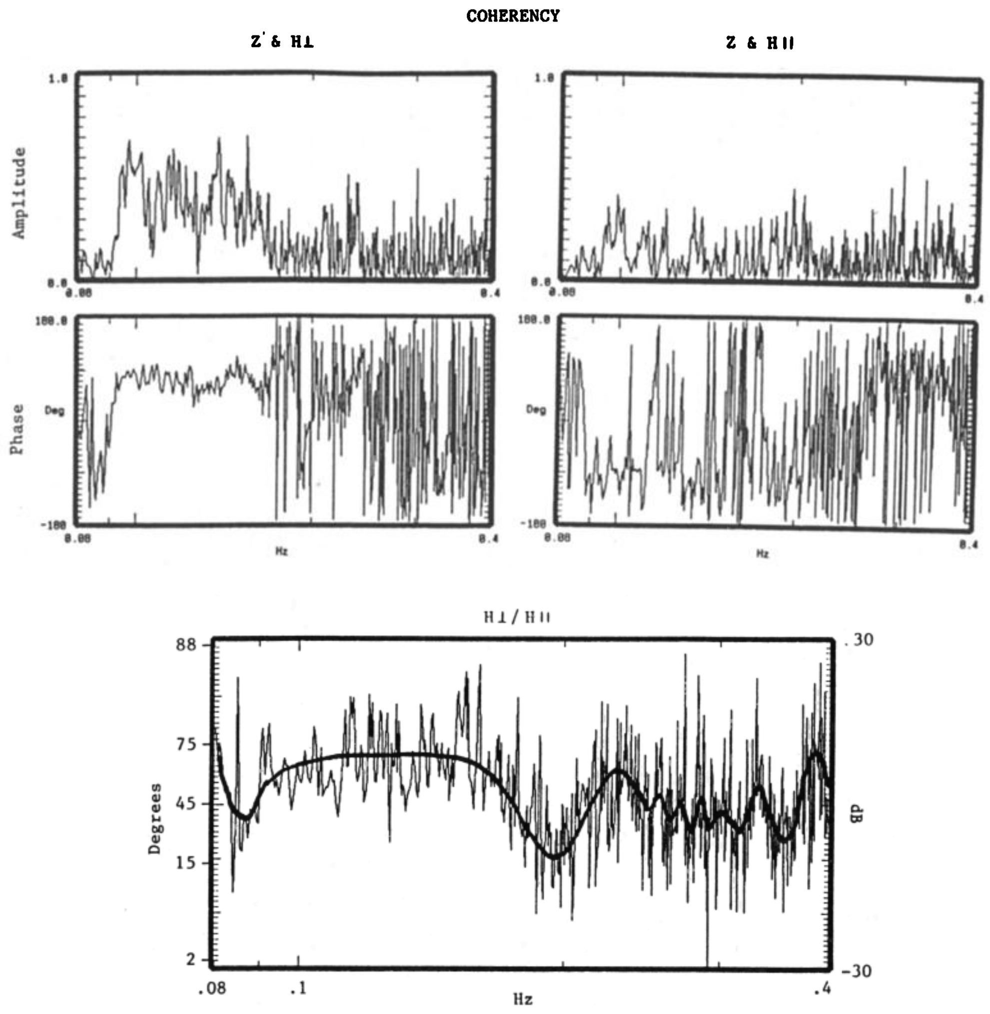

FIG. 9. Coherency between vertical and horizontal motion (13–1600 UT, 12/7) and ratio of the two vertical to horizontal transfer functions. Assuming prograde Rayleigh motion, stable + or − $\pi/2$ phase identifies the proper quadrant of approach and $\tan^{-1}(H\perp/H\|)$ gives the angle from $H\|$.

ACKNOWLEDGMENTS

We gratefully acknowledge Lamont-Doherty Geologic Observatory for providing the original data, and Hugh Bradner, Leroy Dorman, Paul Pomeroy, and Jerry Carter for their interest and useful comments regarding this research. The Office of Naval Research supported this research under Contract No. N00014-86-C-0570.

Auld, B., Latham, G., Nowroozi, A. A., and Seeber, L. (**1969**). "Seismicity off the coast of northern California determined from ocean bottom seismic measurements," Bull. Seism. Soc. Am. **59**, 2001–2015.

Barstow, N., Sutton, G. H., and Carter, J. A. (**1989**). "Particle motion and pressure relationships of ocean bottom noise at 3900 m depth: 0.003 to 5 Hz," Geophys. Res. Lett. **16**, 1185–1188.

Bradner, H. (**1963**). "Probing sea-bottom sediments with microseismic noise," J. Geophys. Res. **68**, 1788–1791.

Bradner, H., and Latham, G. V. (**1972**). "Prograde Rayleigh waves and microseism sources," J. Geophys. Rev. **77**, 6422–6426.

Cessaro, R., and Chan, W. (**1989**). "Wide-angle triangulation array study of simultaneous primary microseism sources," J. Geophys. Res. **94**, 15555–15564.

Cox, C., Deaton, T., and Webb, S. (**1984**). "A deep-sea differential pressure gauge," Atmos. Ocean. Technol. **1** (3), 237–246.

Haubrich, R. A., and McCamy, R. L. (**1963**). "Microseisms: coastal and pelagic sources," Rev. Geophys. **7**, 539–572.

Latham, G. V., and Nowroozi, A. A. (**1968**). "Waves, weather, and ocean bottom microseisms," J. Geophys. Res. **73**, 3945–3956.

Mariners' Weather Log. (**1968**). *U.S. Dept. of Commerce, NOAA, Environmental Data Source* (U.S. Government Printing Office, Washington, DC).

Nowrozzi, A. A., Ewing, M., Nafe, J., and Fliegel, M. (**1968**). "Deep ocean current and its correlation with the ocean tide off the coast of northern California," J. Geophys. Res. **73**, 1921–1932.

Nowroozi, A. A., Kuo, J., and Ewing, M. (**1969**). "Solid earth and oceanic tides recorded on the ocean floor off the coast of northern California," J. Geophys. Res. **74**, 605–614.

Oliver, J. (**1962**). "A worldwide storm of microseisms with periods of about 27 seconds," Bull. Seism. Soc. Am. **52**, 507–518.

Oliver, J., and Page, R. (**1963**). "Concurrent storms of long and ultralong period microseisms," Bull. Seism. Soc. Am. **53**, 15–26.

Piermattei, R., and Nowroozi, A. A. (**1969**). "Dispersion of Rayleigh waves for purely oceanic paths in the Pacific," Bull. Seism. Soc. Am. **59**, 1905–1925.

Sutton, G. H., McDonald, W. G., Prentiss, D. D., and Thanos, S. N. (**1965**). "Ocean-bottom seismic observatories," Proc. IEEE **53** (12), 1909–1921.

Sutton, G. H., Maynard, G. L., and Hussong, D. M. (**1971**). "Widespread occurrence of a high-velocity basal layer in the Pacific crust found with repetitive sources and sonobouys," *The Structure and Physical Properties of the Earth's Crust*, edited by John G. Heacock (Am. Geophys. Union, Washington, DC), pp. 193–209.

Sutton, G. H. (**1986**). "Ocean bottom seismology: history and current status," in *Ocean Seismo-acoustics*, edited by T. Akal and J. M. Berkson (Plenum, New York), pp. 821–844.

Sutton, G. H., and Duennebier, F. K. (**1987**). "Optimum design of ocean bottom seismometers," Marine Geophys. Res. **9**, 47–65.

Sutton, G. H., and Duennebier, F. K. (**1989**). "Avoiding signal distortion and excess noise in OBS;" in *Proceedings of Workshop on Exploration of Deep Continental Margin Crust with Closely Spaced Shots and Receivers,* edited by M. Talwani, P. L. Stoffa, and W. D. Mooney (Houston Area Research Center, The Woodlands, Texas), pp. A21–A22 (with 4 pp. of figures).

Webb, S. C., and Constable, S. C. (**1986**). "Microseism propagation between two sites on the deep seafloor," Bull. Seism. Soc. Am. **76**, 1433–1446.

Webb, S. C., and Cox, C. S. (**1986**). "Observations and modeling of seafloor microseisms," J. Geophys. Res. **91**, 7343–7358.

Webb, S. C. (**1988**). "Long-period acoustic and seismic measurements and ocean floor currents," J. Ocean. Eng. **13**, 263–270.

Yamamoto, T., and Torii, T. (**1986**). "Seabed shear modulus profile inversion using surface gravity (water) wave-induced bottom motion," Geophys. J. R. Astr. Soc. **85**, 413–431.